https://doi.org/10.5194/wes-2023-137
Preprint. Discussion started: 2 November 2023

eawe european academy of wind energy
Open Access WIND ENERGY SCIENCE DISCUSSIONS

Assessing the impact of waves and platform dynamics on floating wind turbine energy production

Alessandro Fontanella[1], Giorgio Colpani[1], Marco De Pascali[1], Sara Muggiasca[1], and Marco Belloli[1]
[1]Mechanical Engineering Department, Politecnico di Milano, Milano, Via La Masa 1, 20156, Italy.
Correspondence: Alessandro Fontanella (alessandro.fontanella@polimi.it)

Abstract. Waves have the potential to increase the power output of a floating wind turbine forcing the rotor to move against wind. Starting from this observation, we use four multi-physics models of increasing complexity to investigate the role of waves and platform movements in the energy conversion process of four floating wind turbines of 5-15 MW in the Mediterranean Sea. The current technology of spar and semi-submersible floating wind turbines is not suitable to exploit the energy of waves because their design philosophy aims to minimize motions and structural loads, whereas large along-wind rotor movements are needed to increase the power output. Instead, in a realistic met-ocean environment, the power curve of the floating wind turbines we analyzed is lower than with a fixed foundation, with AEP reductions of 1.5-2.5%. The lower energy production is mainly ascribed to the platform static tilt, which reduces the rotor area projection on the vertical plane, and to floating-specific features of the turbine controller, that are thought to mitigate structural loading sacrificing performance.

1 Introduction

Floating offshore wind turbines (FOWTs) have a high energy generation potential for deep waters. Compared to their bottom-fixed counterparts they can be installed in more sea areas and further away from the coast, where wind generally blows stronger, while reducing the visual impact from shore and interfering less with other users of the marine space. At the time of writing, the cost of energy produced by floating wind turbines is still high, but in the next decades it is expected to drop to the same level of other wind technologies (Wiser et al. (2021)).

One reason for the higher cost is that advantages of floating wind turbines are balanced by higher system complexity compared bottom-fixed offshore wind turbines. The primary dissimilarity between the two technologies is the compliance of the floating foundation which allows large-amplitude low-frequency motions of the structure. Due to these motions, the rotor of a floating wind turbine may operate differently than when the tower is fixed to the seabed, and it is reasonable to expect this has some effects on power production.

From an energetic point of view, waves driving the floater motion introduce additional energy into the wind turbine which can potentially increase power generation; finding ways to exploit waves energy in floating wind turbines has been identified as one research challenge for the wind energy community (van Kuik et al. (2016)). Few articles exist that study the impact of waves and platform dynamics on the power production of a floating wind turbine. Martini et al. (2016) investigated the effect of met-ocean conditions on tower inclination and hub acceleration and the possible consequences on shutdowns and capacity

https://doi.org/10.5194/wes-2023-137
Preprint. Discussion started: 2 November 2023

eawe european academy of wind energy
Open Access WIND ENERGY SCIENCE DISCUSSIONS

factor. The influence of platform motion on the energy conversion process has been recently approached by Amaral et al. (2022) and Cottura et al. (2022), but both used simplifications such as prescribed sinusoidal movement of the platform in one direction and steady wind, that make their findings difficult to apply to a real scenario.

Knowledge of the influence of waves and platform dynamics on the wind turbine energy production complements results of studies about the effect of wind and atmospheric conditions on the power output of land-based wind turbines. Among these, Clifton et al. (2014) discussed the impact of wind parameters on the performance of a wind turbine installed in a mountain pass with complex inflows, and St. Martin et al. (2016) explored the sensitivity to atmospheric conditions of the power curve and annual energy production of a 1.5MW wind turbine.

The fundamental question this article wants to answer is how the peculiar dynamics of floating foundations and wave excitation impact the energy production of a floating wind turbine. When answering this question, we examine four realistic wind turbine concepts of 5-15MW rating with spar and semi-submersible platforms and we consider the environmental conditions of an area in the Mediterranean sea suitable for the development of floating wind projects. The main contributions of this work are:

1. we use multi-fidelity models of increasing complexity to clarify how physics of the energy conversion process taking place in floating wind turbines is influenced by platform motion and waves;

2. we do a sensitivity analysis of floating wind turbine characteristics (control strategy, turbine rating, platform typology) and met-ocean conditions (wave spectrum, wind-wave directionality) on the generated power;

3. we define a methodology to study the response, in particular power production, of a floating wind turbine with the wind and waves of a selected sea site. Wind and waves are described by a dataset measured by instruments normally used to characterize the met-ocean environment, such as anemometers and wave buoys.

Results and the methodology of this work can be leveraged in the early phase of floating wind projects to quantify their energy production and reduce the risk of investment. Better knowledge of the energy conversion process can help optimizing the turbines design for the operating conditions expected at a given sea area, thus lowering their cost. Moreover, in a future with high share of floating wind turbines, accurate knowledge of the power generated by these machines will be fundamental for electric grid management.

The structure of the article is as follows. Section 2 presents the four floating wind turbine concepts analyzed in this study, the numerical tools we used to estimate their energy production, the met-ocean conditions considered in the analysis, and the four simulation models. Section 3 reports the results of numerical simulations clarifying the influence of wind turbine control, platform compliance, dynamic platform motion, stochastic wind and waves on the power production of the four floating wind turbines. The article is concluded in Section 4 explaining possible uses of results obtained in this paper and reporting some suggestions for future work.

https://doi.org/10.5194/wes-2023-137
Preprint. Discussion started: 2 November 2023

eawe european academy of wind energy
Open Access WIND ENERGY SCIENCE DISCUSSIONS

2 Methodology

A simple mathematical model is useful to understand the effect of platform motion on the energy production of a floating wind turbine. The aerodynamic power of the rotor is:

$$P_\mathrm{r} = \frac{1}{2}\rho C_P \pi R^2 V^3\,, \tag{1}$$

where ρ is the air density, R the rotor radius, V the wind speed on the rotor, and C_P the power coefficient. The rotor of a floating wind turbine undergoes large motions allowed by the foundation compliance. Assuming this movement is harmonic and in the surge direction, we can replace the wind speed V with the relative wind speed V_r which is influenced by rotor moving against wind. If the wind field is uniform and steady, the apparent wind speed seen by the rotor is:

$$V_\mathrm{r}(t) = U - \omega_\mathrm{m} A_\mathrm{m} \cos(\omega_\mathrm{m} t)\,, \tag{2}$$

where U is the mean wind speed, ω_m the motion circular frequency, and A_m the motion amplitude. Substituting Eq. 2 into Eq. 1:

$$P_\mathrm{r}(t) = \frac{1}{2}\rho C_P \pi R^2 \left(U^3 - 3U^2 \omega_\mathrm{m} A_\mathrm{m} \cos(\omega_\mathrm{m} t) + 3U \big(\omega_\mathrm{m} A_\mathrm{m} \cos(\omega_\mathrm{m} t)\big)^2 - \big(\omega_\mathrm{m} A_\mathrm{m} \cos(\omega_\mathrm{m} t)\big)^3 \right). \tag{3}$$

Looking at the four terms inside brackets on the left hand side of Eq. 3 we see that: U^3 is constant in time, $3U^2\omega_\mathrm{m} A_\mathrm{m} \cos(\omega_\mathrm{m} t)$ has a null integral over one period of motion, the same is true for $3\big(\omega_\mathrm{m} A_\mathrm{m} \cos(\omega_\mathrm{m} t)\big)^3$, but not for $U\big(\omega_\mathrm{m} A_\mathrm{m} \cos(\omega_\mathrm{m} t)\big)^2$. The mean value of rotor power over one period of motion is evaluated from Eq. 3 and it is:

$$\overline{P}_\mathrm{r} = \frac{1}{2}\rho C_P \pi R^2 \left(U^3 + \frac{3U A_\mathrm{m}^2 \omega_\mathrm{m}^2}{2} \right). \tag{4}$$

Assuming C_P is constant in time, Eq. 4 shows that in a wind turbine experiencing harmonic platform surge motion the mean power available at rotor is higher than with a fixed foundation. It has to be seen if the power increment predicted by this simple model translates into higher generated power also in normal operating conditions. In fact, the rotor C_P is not constant but it is modified dynamically by the wind turbine controller; moreover, the motion of a floating turbine is not perfectly aligned to the wind, but its direction depends on the directionality of wind and waves and on platform characteristics.

In this work, we assume the energy production of a floating wind turbine is influenced by:

- wind, described by mean wind speed, mean direction, turbulence intensity, and vertical shear.
- wave, described by elevation, period, and direction.
- floater characteristics such as restoring, static stability, dynamic response to environmental loads.
- turbine control strategy, which is modified to accomodate large low-frequency motions permitted by floating foundations and constitutes a key element of difference between floating and bottom-fixed wind turbines (van der Veen et al. (2012)).

In order to isolate their effect, we introduce gradually these parameters in the analysis, assessing the FOWT energy production with scenarios of different levels of complexity.

https://doi.org/10.5194/wes-2023-137
Preprint. Discussion started: 2 November 2023

eawe european academy of wind energy
Open Access WIND ENERGY SCIENCE DISCUSSIONS

2.1 Simulation scenarios and tools

The impact of waves and platform dynamics on power production is studied with four multi-fidelity models of the floating wind turbine and of the wind-wave conditions around it. The four models gradually add complexity to the simple analytical model of Eq. 3; this is shown in Fig. 1. The Harm-M model extends the results of Eq. 3 using a more accurate representation of the wind turbine and its control system. The rotor aerodynamic response is calculated with a non-linear engineering model rather with a constant power coefficient, blades and tower are flexible elements and the wind turbine is regulated with an active control scheme. The turbine is subjected to prescribed harmonic platform motion in different directions and wind is steady and uniform. The Harm-W model introduces in the analysis the hydrodynamic loading and the floater dynamic response to waves; waves are of regular type and can have a different direction than wind. In the Coupled-S model, wind and wave properties are defined according to the standard industrial practice to reflect the met-ocean conditions of a sea area in the Mediterranean; wind and waves are aligned to the platform main axis and excite motion of the rotor in the along wind direction, as in Eq. 3. In the Coupled-C model, the environmental conditions are extracted by means of a clustering algorithm from a database of met-ocean data recorded at the site of reference. In Coupled-C simulations wind and waves are not aligned, but their directionality is representative of the portion of sea of our interest. In this work, the Coupled-C scenario is the most accurate representation of conditions a floating wind turbine would meet if installed in the area we selected.

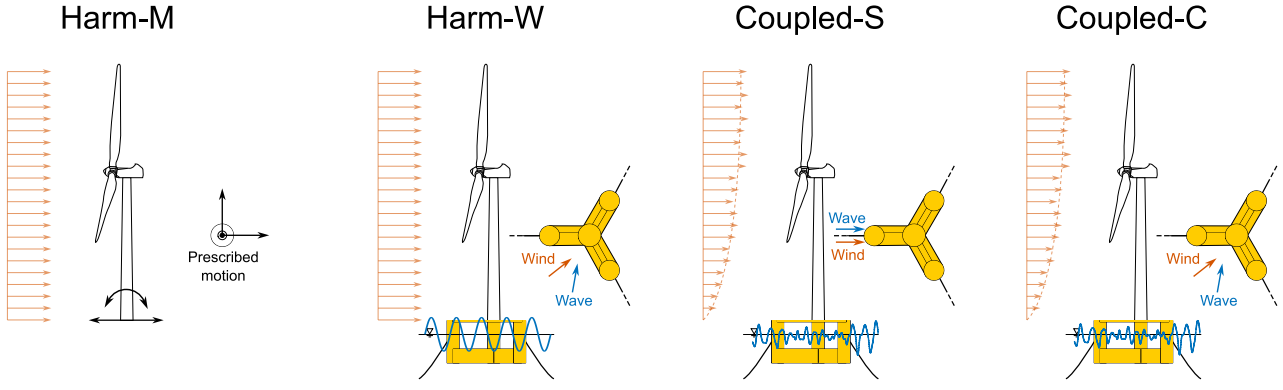

Figure 1. The influence of platform motion due to waves on the power production of floating wind turbines is studied with four simulation scenarios. In the Harm-M case, sinusoidal motion of varying amplitude and frequency is prescribed at the wind turbine tower base. In the Harm-W simulations, the turbine is excited with regular waves of different amplitudes, frequencies and directions. In the coupled simulations, the wind turbine response is computed for several environmental conditions with full-field turbulent wind and irregular waves; wind-wave conditions are obtained with simplifications typically used by standards (Coupled-S) or they are extracted by means of clustering from a database of met-ocean data (Coupled-C).

https://doi.org/10.5194/wes-2023-137
Preprint. Discussion started: 2 November 2023

eawe european academy of wind energy
Open Access WIND ENERGY SCIENCE DISCUSSIONS

The Harm-W and Coupled-C models consider the wind-wave directionality. The wind and waves heading directions (θ and β, respectively) are defined in Fig. 2; their difference $\gamma = \theta - \beta$ is the wind-wave misalignment angle. We assume the nacelle yaw angle is always consistent with the wind direction.

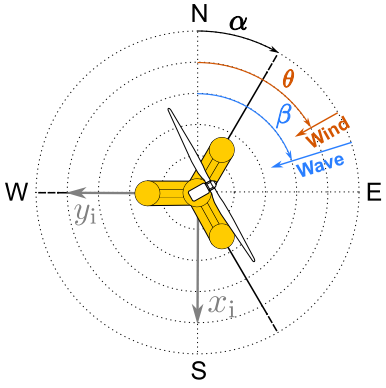

Figure 2. Definition of the platform mounting orientation (α), of the wind direction (θ), the wave direction (β), and the wind-wave misalignment angle ($\gamma = \theta - \beta$). x_i and y_i are the axes of the earth-fixed coordinate system.

All models are built in OpenFAST, which includes different modules for aerodynamics, hydrodynamics, control, and structural dynamics. The aerodynamic forces are calculated in AeroDyn v15 based on the quasi-steady blade element momentum theory. The aerodynamic influence of the tower is accounted with a potential flow model and the blade airfoil aerodynamics is computed using the Beddos-Leishman model. The structural response of the system is modeled in ElastoDyn based on the modal approach. Hydrodynamic forces are calculated in HydroDyn using a combination of potential-flow theory and strip-theory solution; the hydrodynamic coefficients required for the potential-flow solution are obtained with a panel code (e.g., WAMIT). The mooring lines are modeled in MoorDyn which uses a lumped-mass approach to discretize the cable dynamics over the length of the lines.

The incoming turbulent wind is introduced in the simulations by means of TurbSim, which is a stochastic, full-field, turbulent wind simulator using a statistical model to numerically simulate the time series of the three components of the wind velocity vector at specified points of a two-dimensional grid fixed in space.

2.1.1 Simulations with prescribed motion

In this scenario platform motion is prescribed at tower base, it is sinusoidal and along one of the six rigid-body motion directions of the turbine foundation. The motion frequency ranges from 0 Hz to 0.3 Hz; the motion amplitude varies from 0 m to 3 m in case of translations, and from 0° to 1.25° in case of rotations; wind is steady and has no shear.

The outcome of Harm-M simulations is the MPRO function, first introduced by Amaral et al. (2022), mapping the turbine average power $\overline{P_g}$ to the tower-base motion amplitude A_m and frequency f_m for a given wind speed U:

$$f_{\mathrm{MPRO}} : \{U, A_m, f_m\} \rightarrow \overline{P_g}. \tag{5}$$

https://doi.org/10.5194/wes-2023-137
Preprint. Discussion started: 2 November 2023

eawe european academy of wind energy
Open Access WIND ENERGY SCIENCE DISCUSSIONS

The MPRO function is computed at discrete points based on time series of the turbine generated power from OpenFAST simulations.

2.1.2 Simulations with regular waves

The Harm-W scenario is similar to the Harm-M, but introduces in the analysis the dynamic response of the floating wind turbine to incident wave. Wave is of regular type, the height ranges from 0.05 m to 3 m and the frequency from 0.05 Hz to 0.3 Hz. These values are representative of the wave conditions at the sea site of reference, described in Sect. 2.3. Wind is steady and has no shear.

We summarize the results of the Harm-W case with a function mapping the turbine average power to the wave amplitude A_{w}, frequency f_{w}, and direction β for a given wind speed:

$$f_{\mathrm{WPRO}} : \{U, A_{\mathrm{w}}, f_{\mathrm{w}}, \beta\} \rightarrow \overline{P_{\mathrm{g}}}. \tag{6}$$

The WPRO function is defined at discrete points from time series of the turbine power output that are obtained in OpenFAST.

2.1.3 Coupled simulation with simplified wind-wave conditions

The Coupled-S model uses stochastic wind and waves. The load cases are defined according to the recommendations of IEC 61400-3 (International Electrotechnical Commission (2019)) for fatigue load calculations:

- wind and wave are aligned to the platform symmetry axis (i.e., with reference to Fig. 2, $\alpha = \beta = \theta = 0°$);
- a wind speed interval of 2 m/s is considered starting from 3 m/s and up to 25 m/s;
- the wave height is defined from the linear correlation law with average wind speed;
- three wave periods are associated to each wave height. Wave periods are obtained from the scatter diagram of the site as the three most probable for the selected wave height.

2.1.4 Coupled simulation with clustered wind-wave conditions

Coupled-C simulations reproduce the wind-wave environment of the sea site of reference without making use of assumptions on the relations among wind speed, wind direction, wave height, wave period, and wave direction. Instead, the load cases of simulations are extracted from long-term series of the wind and wave parameters.

Approximately 4 CPU hours are required to simulate in OpenFAST one sea state for 3 hours, and it is unpractical to simulate a dataset covering several moths or years. Thus, the Coupled-C model considers a small subset of conditions that are representative of the long-term sea conditions at the site. The selection procedure is based on the data-clustering technique, which aims to extract features from the original dataset giving a more compact representation of the dataset properties. Data clustering has seen application in the wave climate analysis (Camus et al. (2011)) and to extrapolate wind statistics needed to estimate the energy production of wind energy systems (Schelbergen et al. (2020)).

https://doi.org/10.5194/wes-2023-137
Preprint. Discussion started: 2 November 2023

eawe european academy of wind energy
Open Access WIND ENERGY SCIENCE DISCUSSIONS

Here, the selection of the subset of met-ocean conditions is based on the K-means algorithm (KMA) (Arthur and Vassilvitskii (2007)). The initial database is formed by five-dimensional vectors, whose elements are the variables of interest that characterize the wind and wave climate: wind speed (U), wind direction (β), wave significant height (H_{s}), wave peak period (T_{p}), and wave direction (θ).

Given the initial database of N five-dimensional vectors $\mathbf{x}^i = \{U_i, \beta_i, H_{\mathrm{s},i}, T_{\mathrm{p},i}, \theta_i\}$ with $i = 1, \ldots, N$, the KMA identifies M groups of data, each defined by a five-dimensional prototype $\mathbf{v}^k$ with $k = 1, \ldots, M$ called centroid. The clustering procedure starts with a random initialization of the M centroids; on each algorithm iteration, the nearest data to each centroid are identified and the centroid is redefined as the mean of the corresponding data. For example, on the $(r+1)$ step, a data vector $\mathbf{x}^i$ is assigned to the group $j|\{\min\|\mathbf{x}^i - \mathbf{v}_r^j\|, j = 1, \ldots, M\}$, where $\|\cdot\|$ is the Euclidean distance, and $\mathbf{v}_r^j$ is the j-th centroid at the r-th step. Once every data vector is assigned to a group, the centroid is updated as:

$$\mathbf{v}_r^j = \sum_{\mathbf{x}^i \in C^j} \frac{\mathbf{x}^i}{n_j} = 1\,, \tag{7}$$

where n_j is the number of elements of the j-th group and C^j is the subset of data included in the group j. The KMA iteratively moves the centroids minimizing the overall within-cluster distance until it converges and data belonging to every group are stabilized. The working principle of the clustering algorithm is showcased in Appendix A using the dataset of the sea site of reference of this study, that is presented in Sect. 2.3.

The number of clusters representing the sea states is a trade-off between the computational cost required to simulate them and the error committed in using a subset of data instead of the complete dataset. Here, the number of clusters is fixed to $M = 36$, which is the same number of conditions considered in the Coupled-S simulations.

2.2 Floating wind turbines concepts

The wind turbines of the FOWTs concepts are the NREL 5 MW (Jonkman et al. (2009)) and the IEA 15 MW (Gaertner et al. (2020)) which key parameters are summarized in Table 1.

https://doi.org/10.5194/wes-2023-137
Preprint. Discussion started: 2 November 2023

eawe european academy of wind energy
Open Access WIND ENERGY SCIENCE DISCUSSIONS

Table 1. Key properties of the NREL 5 MW and IEA 15 MW wind turbines.

Parameter	Unit	NREL 5 MW	IEA 15 MW
Power rating	MW	5	15
Cut-in wind speed	m/s	3	3
Rated wind speed	m/s	11.4	10.59
Cut-out wind speed	m/s	25	25
Design tip-speed ratio	-	7.55	9
Minimum rotor speed	rpm	-	5
Rated rotor speed	rpm	12	7.56
Rotor diameter	m	126	240
Hub height	m	90	150

The two wind turbines have a conventional variable-speed, variable blade-pitch-to-feather configuration. Power-production operation is controlled with the Reference OpenSource Controller (ROSCO) of Abbas et al. (2022) which is deemed to be representative of controllers adopted in commercial multi-megawatt wind turbines. In ROSCO, two active proportional integral (PI) controllers are implemented for generator torque and collective blade pitch angle; saturation limits on rotors speed and blade pitch are used to ensure the turbine works within its design limits. ROSCO has two operating regions:

- below rated wind speed. Blade pitch is fixed to its design value of $0°$, and a PI controller regulates the generator torque to track the design tip-speed ratio (TSR). The IEA 15 MW has a minimum rotors speed constraint of 5 rpm, thus at low wind speed the blade pitch is scheduled based on a wind speed estimate to improve the turbine power output. This functionality is not used in the NREL 5 MW. The estimate of rotor-effective wind speed required by the TSR-tracking controller and the pitch scheduling is provided by an extended Kalman-filter estimator.
- above rated wind speed. Generator torque is constant and equal to its rated value and rotor speed is regulated with a PI controller on the collective blade pitch angle.

In addition to these baseline control strategies, we used two ROSCO functionalities meant to improve the operation of FOWTs:

- peak shaving. This algorithm reduces the maximum thrust force reached when the turbine operates in near-rated winds. The peak shaving is implemented prescribing a minimum blade pitch $> 0°$ function of the wind speed.
- nacelle velocity feedback. In above rated wind speed, the nacelle fore-aft acceleration is band-pass filtered, integrated, and multiplied by a constant gain. The blade pitch command obtained with this algorithm is summed to the output of the PI pitch controller for rotor speed to improve stability of platform motion.

https://doi.org/10.5194/wes-2023-137
Preprint. Discussion started: 2 November 2023

eawe european academy of wind energy
Open Access WIND ENERGY SCIENCE DISCUSSIONS

We avoided using any control algorithm for start-up and shut-down sequences. When wind speed is below cut-in or above cut-out, the wind turbine is stopped and does not produce any power. Moroever, there is no control action to regulate the nacelle-yaw angle, which is assumed to be constant.

The steady-state operating points of the land-based version (i.e., with fixed tower base) of the NREL 5 MW and IEA 15 MW regulated with the control strategy described above are visualized in Fig. 3.

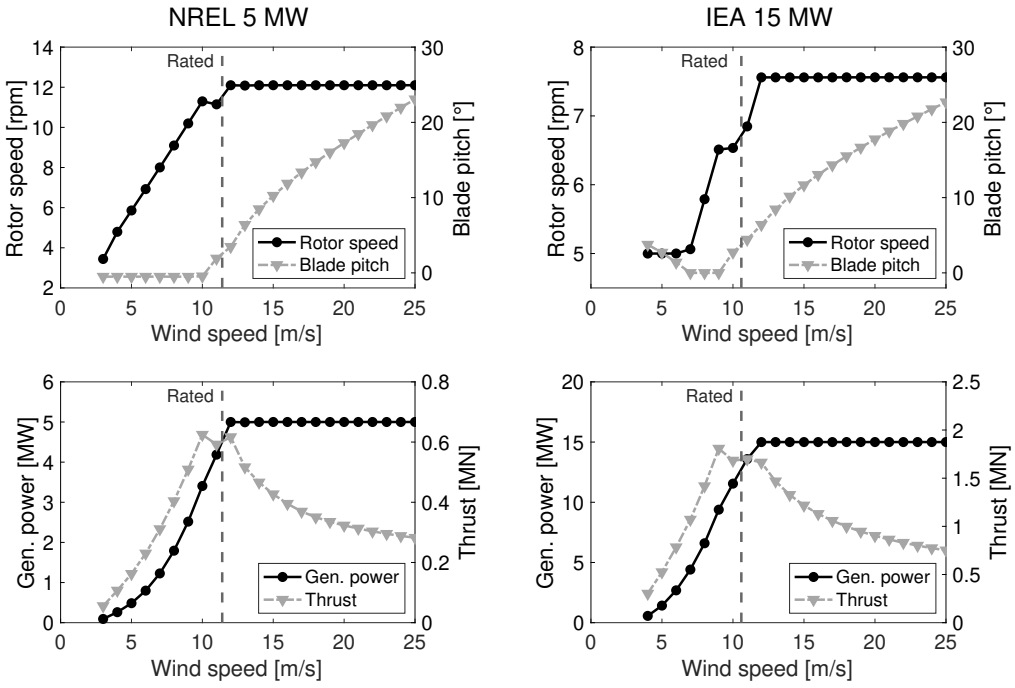

Figure 3. Steady-state operating points of the land-based version of the NREL 5 MW and IEA 15 MW wind turbines.

For each wind turbine two platform concepts are examined: a spar-buoy and a semi-submersible. We decided to focus on these substructures typologies because they have been adopted in recent commercial projects and research works. Moreover, there are OpenFAST models easily accessible in online repositories.

2.2.1 VolturnUS 15 MW semi-submersible

The UMaine (University of Maine) VolturnuUS-S (Allen et al. (2020)) is an open-source concept of a semi-submersible floating wind turbine based on the IEA 15 MW. The floater is made of steel and is composed of three 12.5 m diameter columns disposed symmetrically around a central column hosting the wind turbine. The three bottom pontoons connecting the inner and outer columns have a rectangular section (12.5 $\times$ 7.0 m); three cylindrical struts connect the top of the outer column to the central one. The operational draft of the floater is 20 m; the total mass of the platform is 17854 t. The mooring system is designed for a generic 200-m-depth location and is composed of three 850 m long chain-catenary lines, arranged at 120° angle around the

https://doi.org/10.5194/wes-2023-137
Preprint. Discussion started: 2 November 2023

floater. The fairlead is located at the extreme point of each external column, at a radius of 58 m from the vertical axis of the floater and 14 m below the sea water level.

2.2.2 WindCrete 15 MW spar

The WindCrete, introduced by Campos et al. (2016), is a spar-type platform supporting the IEA 15 MW. The tower and the spar form a monolithic structure made of concrete. The spar has a diameter of 18.6 m, a draft of 155 m, and has ballast in its lower section to increase the hydrostatic stiffness in the roll and pitch directions. The tower has conical shape and, in the version of Campos et al. (2016), it places the hub 135 m above the mean sea level. We modified the tower to have an hub height of 150 m. The mooring system consists of three catenary lines attached to the platform hull with delta-shaped connections. The global response of the WindCrete to several wind and wave is examined by Mahfouz et al. (2021) and the OpenFAST model of the platform is published in the repository of Molins et al. (2020).

2.2.3 DeepCwind 5 MW semi-submersible

The OC4 DeepCwind semi-submersible is a floater design developed in the DeepCwind project (Robertson et al. (2014)). The platform consists of a main column supporting the tower and three offset columns that are connected to the main one through a series of smaller diameter pontoons and cross members; the draft is 20 m. The floater is moored with three catenary lines spread symmetrically about the vertical axis. The fairleads are positioned at a depth of 14.0 m below the water level, at a radius of 40.87 m from the platform centerline, while the anchors are located at a water depth of 200 m and at a radius of 837.6 m from the platform centerline.

2.2.4 OC3 5 MW spar

The OC3-Hywind spar-buoy is a floater designed for the NREL 5 MW reference wind turbine (Jonkman (2009)). The floater is made of steel, ballasted with inert material, and it is composed of a 120 m draft cylinder of 9.4 m diameter, tapered to 6.5 m diameter in correspondence of the sea surface. The linearly tapered conical region extends from a depth of 4 m to a depth of 12 m below the SWL; the overall length of the floater is 130 m. The design water depth for the floater is 320 m. The mooring system consists of three all-chain slack catenaries, spread 120° apart; each line has an unstretched length of 902.2 m and a diameter of 0.09 m; a delta line connecting mooring lines to fairleads is used to increase yaw stiffness.

2.3 Reference sea site and met-ocean conditions

The wind and wave conditions defining the load cases are representative of the climate at a sea area suitable for development of floating wind projects that is sited in the Golf de Fos, located off the French coast in the Mediterranean sea. The site of reference is shown in Fig. 4, it is 40 km offshore Fos Sure Mer and its approximate location is identified by the coordinates Lat. 43°6'15.12"N, Long. 4°44'32.06"E.

https://doi.org/10.5194/wes-2023-137
Preprint. Discussion started: 2 November 2023

eawe european academy of wind energy
Open Access WIND ENERGY SCIENCE DISCUSSIONS

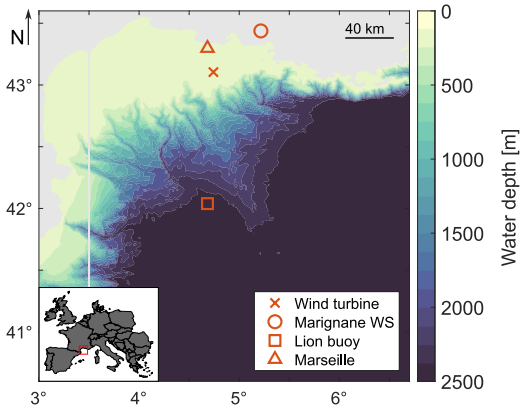

Figure 4. Sea area of the reference site of this study. The area is located in the Mediterranean sea off the French coast, as shown in the inset map. Markers show the position of the floating wind turbine, the Marignane Weather Station, the Lion Buoy, and the city of Marseille. Land is depicted in gray and the color scale corresponds to water depth (EMODnet (2023)).

Two open-access databases have been used to characterize the wind and wave conditions at this site: wind data of the Marignane Weather Station, provided by Meteostat (Meteostat (2022)); wave data of the Gulf of Lion buoy, located 100 km south to the site location, shared by MetoFrance (France (2022)). The variables of interest for this study are: wind speed at 10 m height, wind direction, wave elevation, wave period, wave direction. The two databases contain wind-wave measurements for several years, however, wave directionality measurements are available only for a period of six months, from October 2019 to March 2019. The time resolution is 1 hour; the dataset with simultaneous information about the five variables of interest has 3362 data points in total.

No information about the vertical profile of mean wind speed is available, thus it is assumed to follow the Normal Wind Profile (NWP):

$$U(z) = U(h)\left(\frac{z}{h}\right)^{0.14}, \tag{8}$$

where U is the mean wind speed, z a generic height, and h is the reference height of 10 m.

The wind speed distribution is essential for evaluating the wind turbine annual energy production. Figure 5 shows the probability density function of the 1-hour mean wind speed extrapolated at 150 m height (i.e., the hub height of the IEA 15 MW) by means of Eq. 8. The best fitting Weibull distribution has scale parameter of 7.17 and shape parameter of 1.38. The probability of occurrence of wind speed is over predicted in some bins (e.g., 5-6 m/s, 8-9 m/s), and this problem is likely due to the small size of the database. The best fitting Weibull distribution for the 1-hour mean wind speed at the hub height of the NREL 5 MW (90 m) has scale parameter of 6.68 and shape parameter of 1.38.

https://doi.org/10.5194/wes-2023-137
Preprint. Discussion started: 2 November 2023

eawe european academy of wind energy
Open Access WIND ENERGY SCIENCE DISCUSSIONS

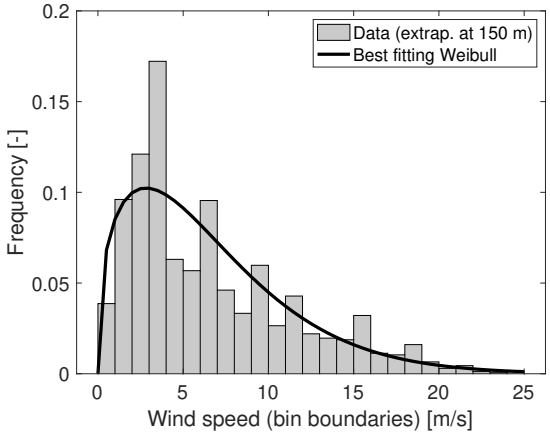

Figure 5. Probability density function of the 1-hour mean wind speed at 150 m at Marignane Weather Station obtained from data recorded between October 2019 and March 2019. The best fitting Weibull distribution is obtained for scale parameter of 7.17 and shape parameter of 1.38.

There is no measurement of turbulence intensity at the site, thus the Normal Turbulence Model (NTM) is used. The characteristic standard deviation of wind speed is given by:

$$\sigma_u = I_{\mathrm{ref}}(0.75U_{150} + 5.6)\,, \tag{9}$$

where U_{150} is the mean wind speed at 150 m, and $I_{\mathrm{ref}} = 0.12$ which is appropriate for onshore Class C turbines and conservative for offshore turbines of similar characteristics.

Figure 6 shows the wind rose from the records, where wind speeds were extrapolated to their value at 150 m by means of Eq. 8, and the rose of the wave coming-from direction. Waves come from SE most of the time, while it is equally probable to have wind from SE and NW, suggesting the assumption of wind-wave alignment is not representative of this site.

In the Coupled-S model, wave elevation H_{s} is assumed to depend linearly on wind speed:

$$H_{\mathrm{s}} = 0.128U_{150} + 0.844\,. \tag{10}$$

Coefficients in the expression were obtained from linear regression of wave height and 150 m-mean wind speed data.

The wind-wave conditions of the Coupled-S simulations for the Golf de Fos site are reported in Table B1. Environmental conditions of the Coupled-C simulations are obtained applying the clustering algorithm of Sect. 2.1.4 to the dataset of five-dimensional vectors $\mathbf{x}^i = \{U_i, \beta_i, H_{\mathrm{s},i}, T_{\mathrm{p},i}, \theta_i\}$ with $i = 1, \ldots, 3362$. The 36 conditions identified by the clustering algorithm are reported in Table B2.

https://doi.org/10.5194/wes-2023-137
Preprint. Discussion started: 2 November 2023

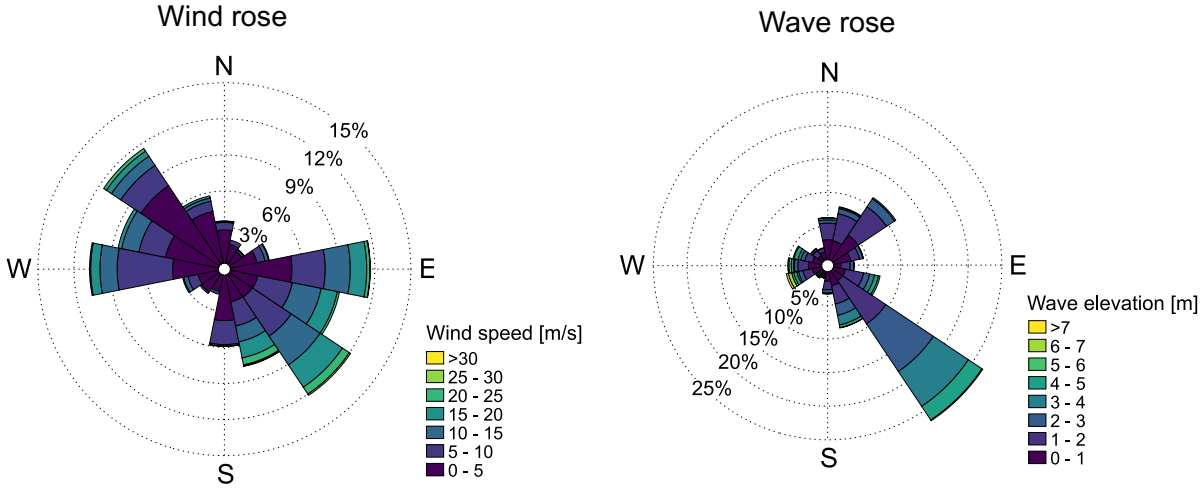

Figure 6. Wind rose of the 1-hour wind speed at 150 m and wave rose of the 1-hour wave elevation.

3 Results

3.1 Influence of wind turbine control and platform static tilt

The wind turbine control strategy and the floater static tilt influence the steady-state power production of a floating wind turbine. Figure 7 shows how the power curve of the NREL 5 MW and the IEA 15 MW with steady non-sheared wind changes due to the use of a peak-shaving routine in the wind turbine controller and due to a floating foundation compared to a bottom-fixed one. The peak shaving routine reduces the turbine power near the rated wind speed because the turbine does not work at the power-optimal operating point when blade pitch is different than the fine pitch. This reduction is up to 8.9% for the NREL 5 MW and 11% for the IEA 15 MW.

When the turbine is on top of a floating foundation, the thrust force results in a static tilt rotation of the structure and a reduction of the rotor area projection on the vertical plane. The four floating wind turbines have a maximum static tilt between 3-4° near the rated wind speed and this result in a maximum reduction of the generated power around 3%.

https://doi.org/10.5194/wes-2023-137
Preprint. Discussion started: 2 November 2023

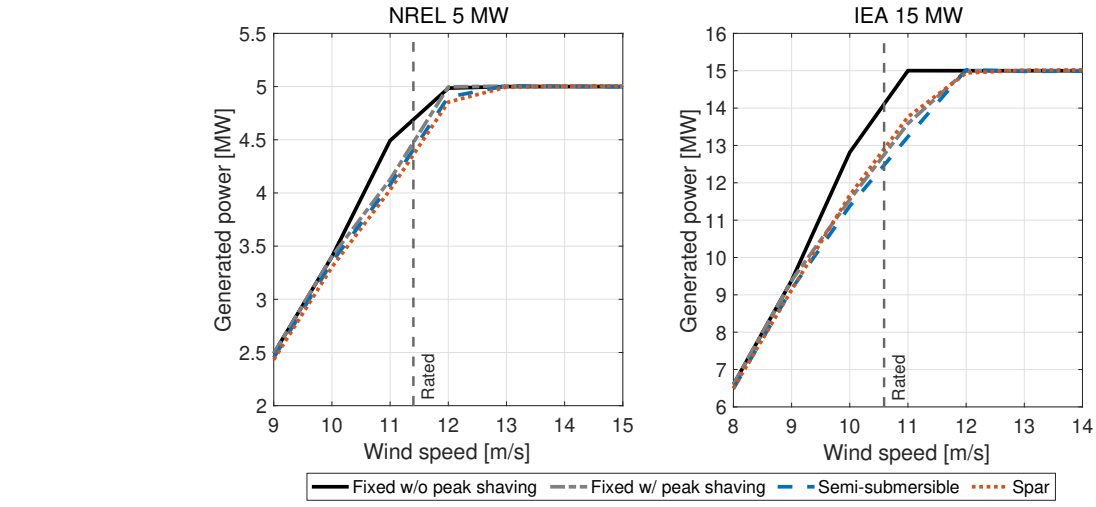

Figure 7. Steady-state power curves of the NREL 5 MW and IEA 15 MW wind turbines with a fixed, a semi-submersible, and a spar foundations. The power curve near the rated wind speed is influenced by the peak shaving control strategy, which reduces the conversion efficiency making the turbine work far from its aerodynamically-optimal operating point, and the use of a floating foundation, which is responsible of a large rotor tilt angle and a consequent reduction of the rotor area projection on the plane normal to wind. Peak shaving is used in all floating wind turbines.

3.2 Sensitivity to wind shear and turbulence

The met-ocean database at our disposal does not provide any information about the vertical profile of mean wind speed and turbulence intensity. Therefore wind shear and turbulence in Coupled-S and Coupled-C simulations have been selected based on standards. This procedure is common in the early stage of floating offshore wind projects, when detailed measurements of wind parameters at a given site are not available. Figure 8 shows how the power curve of the IEA 15 MW on the VolturnUS changes for several values of the wind shear exponent and turbulence intensity.

Sensitivity to wind shear is assessed from the power curve with steady wind and no waves. The wind speed vertical profile is obtained with Eq. 8 fixing the reference at 150 m and changing the shear exponent α. The shear exponent influences the wind turbine power curve in the below rated region: the rotor-averaged wind speed decreases for higher values of α and the turbine produces less power; above the rated wind speed, the turbine power is saturated and it is not affected by α.

Sensitivity to turbulence intensity is evaluated simulating the wind turbine with no waves, the wind speeds of Table B1 and changing I_{ref} in the NTM of Eq. 9. In Fig. 8 we see that in the case with $I_{\mathrm{ref}} = 6\%$ the power is higher than with $I_{\mathrm{ref}} = 0\%$ for near-rated wind speeds. A further increase in turbulence brings higher power near cut-in and lower power close to rated.

https://doi.org/10.5194/wes-2023-137
Preprint. Discussion started: 2 November 2023

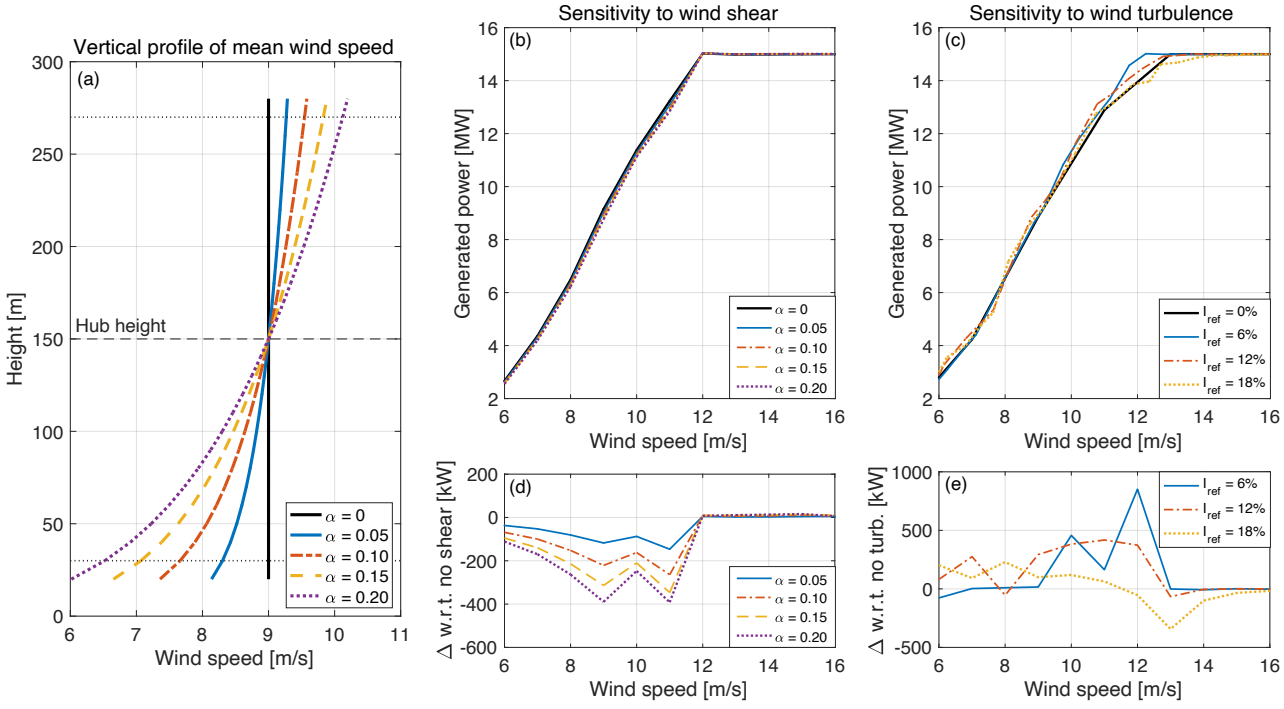

Figure 8. Sensitivity to wind shear and turbulence intensity of the VolturnUS. **(a)** Vertical profile of mean wind speed with different values of the wind shear exponent (α). **(b)** power curve with steady wind and five values of α. **(d)** variation of the power curve with respect to the case with no shear ($\alpha = 0$). **(c)** power curve with four values of the reference turbulence intensity (I_{ref}). **(e)** variation of the power curve from the case with steady wind ($I_{\mathrm{ref}} = 0\%$).

3.3 Power response to prescribed platform motion

Figure 9 shows the time series of power generated by the IEA 15 MW in the Harm-M scenario, with prescribed surge motion of 1.5 m amplitude and 0.2 Hz frequency. Two steady-uniform wind conditions are examined, one in the below-rated region with a wind speed of 9 m/s, and one with with above-rated wind speed of 15 m/s. In the 9 m/s case, the land-based turbine has an average production of 9.4 MW, which is increased to 10.1 MW when the platform undergoes harmonic surge motion (+7.5%). In the above rated operating condition, motion has a lower influence on the power production that passes from 15 MW of the land-based turbine to 14.9 MW when the platform moves (-1%).

Figure 10 shows the MPRO function of the IEA 15 MW computed from results of Harm-M simulations, considering surge and pitch motions and a wind speed of 9 m/s; f_{MPRO} in Fig. 10 is normalized by the turbine power with no prescribed motion. The turbine has a static pitch angle of 3.4°, corresponding to the platform tilt rotation of the VolturnUS at 9 m/s. The average power output increases with increasing frequency and amplitude of platform motion. Movement in the surge or pitch directions gives an apparent wind at the rotor, which causes an increase in generated power, as explained in the simple analytical model

https://doi.org/10.5194/wes-2023-137
Preprint. Discussion started: 2 November 2023

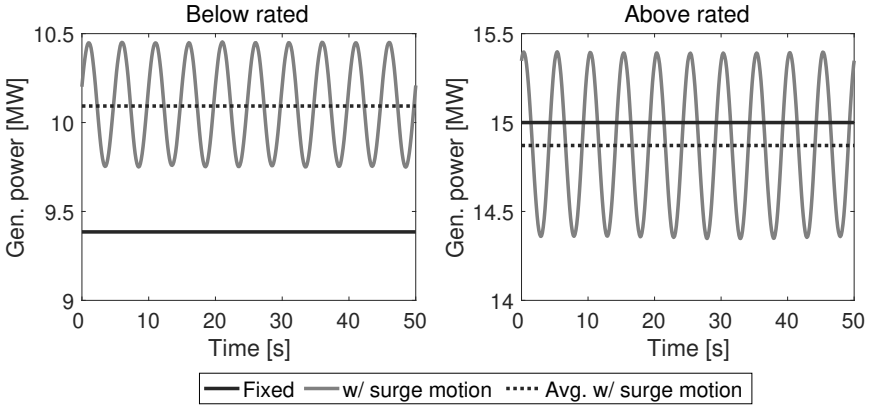

Figure 9. Power generated by the IEA 15 MW with a below-rated wind speed of 9 m/s and an above-rated wind speed of 15 m/s, in the land-based configuration and with prescribed platform surge motion of 1.5 m amplitude and 0.2 Hz frequency.

of Eq. 3. The power increment is proportional to the amplitude of the apparent wind speed variations at hub, which is equal to $U_{\mathrm{r,h}} = \omega_{\mathrm{m}} A_{\mathrm{m}}$ in case of surge and $U_{\mathrm{r,h}} = \omega_{\mathrm{m}} A_{\mathrm{m}} h_{\mathrm{h}}$ in case of pitch, where h_{h} is the hub height. In the surge case the apparent wind is uniform across the rotor and equal to $U_{\mathrm{r,h}}$, whereas in the pitch case it is higher than $U_{\mathrm{r,h}}$ in the upper portion of the rotor disk and lower in the lower portion. If we compare cases of surge and pitch motion with similar $U_{\mathrm{r,h}}$, the mean power is slightly higher in case of pitch motion and this is attributed to the higher amplitude of wind speed oscillations in the upper part of the rotor.

The average power output in the above rated region is slightly lower than the turbine rated power regardless of the tower base motion: with the amplitude-frequency combinations of Fig. 10, the average generated power is between 14.867 MW and 14.877 MW. Platform motion in the sway, heave, roll, and yaw directions does not produce any noticeable increase in generated power.

Harm-M simulations show a wind turbine operating at a below-rated wind speed produces more power if the rotor moves cyclically in the wind direction and the increment is due to the energy in the apparent wind. This is in agreement with the analytical model of Eq. 3 and with results of Amaral et al. (2022) and Cottura et al. (2022) obtained with comparable approaches. According to results of the Harm-M simulations, platform motion driven by wave excitation can bring a meaningful increment of the generated power. However, with Harm-W, Coupled-S and Coupled-C simulations we will show these gains are not achieved in normal operating conditions.

3.4 Power response with regular waves

Results of the Harm-W simulations are summarized with the WPRO function. The WPRO functions for the four platforms, with wind and waves aligned to the platform main axis and a wind speed of 9 m/s are reported in Fig. 11. We see that wave excitation increases the generated power in all platforms, the 5 MW spar has the largest increment and the 15 MW semi-

https://doi.org/10.5194/wes-2023-137
Preprint. Discussion started: 2 November 2023

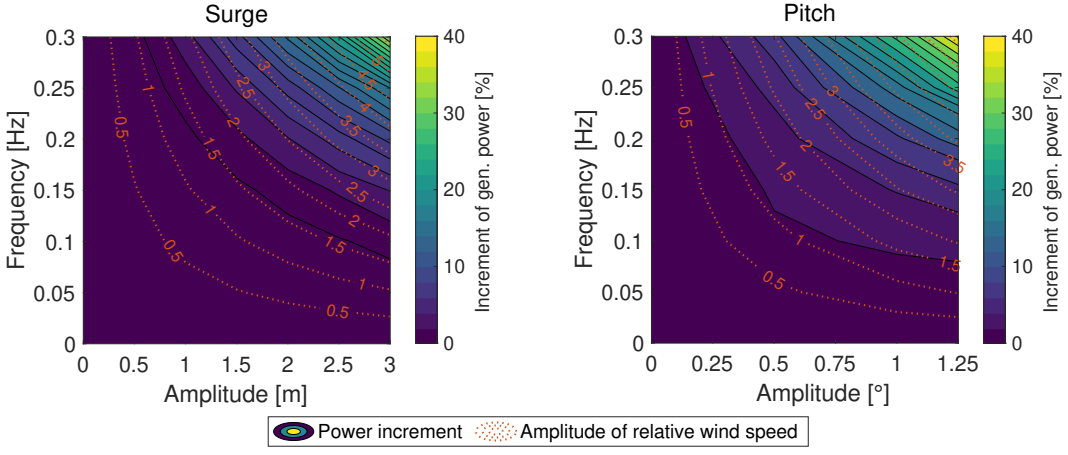

Figure 10. Increment of generated power of the IEA 15 MW with prescribed motion in the platform surge and pitch directions and a below rated wind speed of 9 m/s. "Power increment" is the motion power response operator function (f_{MPRO}) normalized by the turbine power with no prescribed motion. The "amplitude of relative wind speed" is the amplitude of the apparent wind speed at hub due to platform motion ($U_{\mathrm{r,h}}$).

submersible has the smallest. In all turbines the power increment is proportional to wave amplitude. In first approximation, platform motion due to wave excitation is linearly proportional to wave height, thus bigger waves cause larger motions in the along-wind direction which cause the higher mean power output with the mechanism explained in Eq. 3 and with the Harm-M simulations.

Except the for VolturnUS, for a given wave amplitude the power increment is inversely proportional to wave frequency. This result, which appears to be in contradiction with Harm-M results, is justified when taking into account the dynamic response of the platform to wave excitation. Lower-frequency waves excite the FOWTs closer to their natural frequencies, resulting in larger movements. Large high-frequency motions that would lead to significant gains in the turbine power output are not possible due to the floaters design preventing the platform modes from being excited in resonance by waves. In the 15 MW semi-submersible case, the maximum power increment is at 0.1 Hz due to the platform hydrodynamic characteristics.

In the Harm-W analysis, the 5 MW spar wind turbine has the largest increment of generated power, that reaches almost 10% with a wave amplitude of 3 m at 0.05 Hz. This large increment, which is not seen in other platforms, is likely due to the coupled surge and pitch motions that occur at relatively high frequency and involves large movements. The surge motion with 3 m waves of 0.05 Hz frequency is over 3 m of amplitude for the 5 MW spar, whereas it is lower than 1 m in all other turbines. Comparing the WPRO for the two turbine sizes and for the same floater type, we see that power gains for the 5 MW turbines are generally higher than for their 15 MW counterparts. This is due to the fact that platform modes are at lower frequency in the 15 MW turbines and motion due to first-order wave loads is milder.

https://doi.org/10.5194/wes-2023-137
Preprint. Discussion started: 2 November 2023

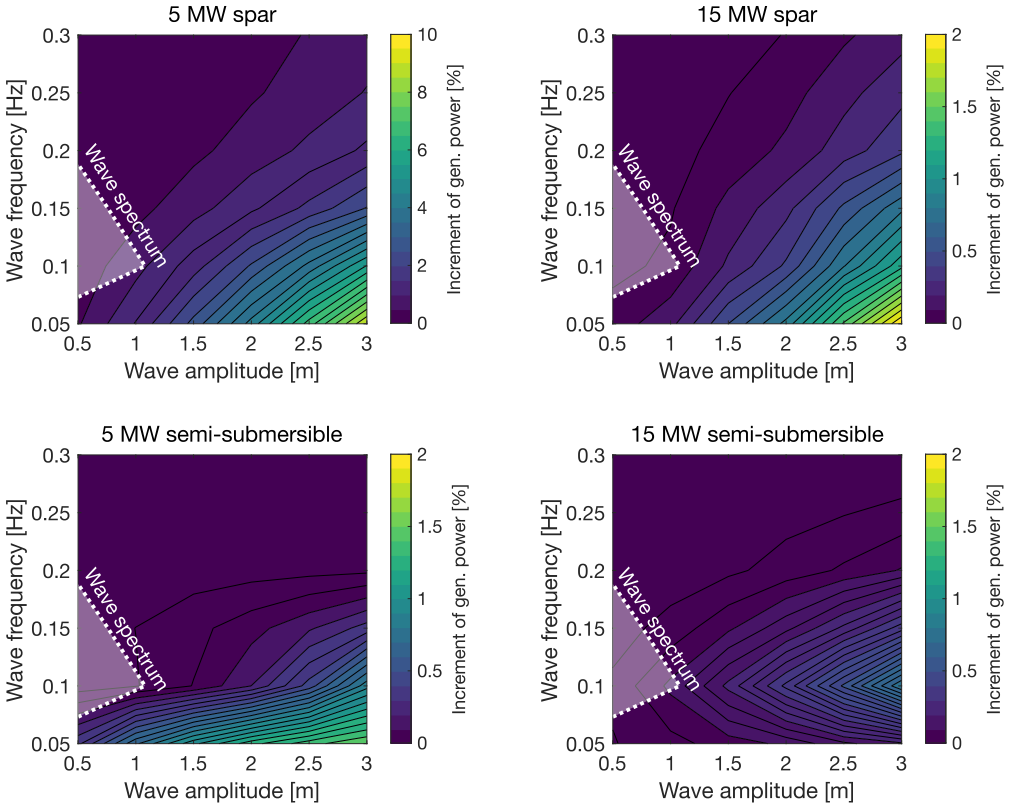

Figure 11. Wave power response operator function (f_{WPRO}) of the four floating wind turbines with wind and waves aligned to the platform main axis, with a below rated wind speed of 9 m/s. The dashed area is in correspondence of the wave spectrum with H_{s} = 4 m and T_{p} = 9 s. The f_{WPRO} in the figure is normalized by the turbine power with no waves.

Figure 11 shows that low-frequency waves can increase the power output of floating wind turbines. However, these power gains are achieved in a real scenario if waves with these characteristics exist. The dashed area in Fig. 11 is in correspondence of a wave spectrum that can occur at the Golf de Fos site. The wave spectrum is obtained from the wave height PSD, computed according to the JONSWAP model of Hasselmann et al. (1973) with H_{s} = 4 m and T_{p} = 9 s. This is the most severe sea state recorded in the dataset at our disposal and has rather high waves of low period, which is the condition required to increase power production. As visible, wave excitation is not powerful enough to generate a meaningful increase of the generated power. Depending on the installation site, it is possible that during its lifetime the floater may encounter a harsher sea, but the probability of occurrence at wind speeds lower than rated is generally low.

To investigate the influence of wind-wave directionality, we calculated the f_{WPRO} of the VolturnUS for a below rated wind speed of 9 m/s, regular waves of 0.1 Hz frequency and wave coming-from direction $\beta = [0°, 30°, 60°, 90°, 120°]$, while $\alpha = \theta = 0°$ always. The result is reported in Fig. 12: the largest power output gain is achieved when wind and waves are aligned, because wave forces the platform to move in the wind direction. Conversely, when wave is perpendicular to wind, motions in the sway

https://doi.org/10.5194/wes-2023-137
Preprint. Discussion started: 2 November 2023

eawe european academy of wind energy
Open Access WIND ENERGY SCIENCE DISCUSSIONS

and roll directions are excited and these have a negligible effect on the generated power. The trend is confirmed for three values of wave amplitude and a similar result is obtained with waves of 0.05 Hz frequency (not shown here for brevity).

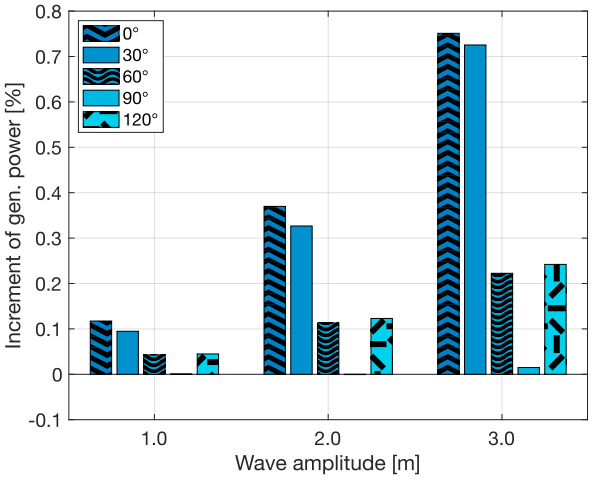

Figure 12. Increment of generated power of the VolturnUS due to harmonic waves with a below rated wind speed of 9 m/s, regular waves of 0.1 Hz frequency and five values of the misalignment angle $(\theta - \beta)$.

Simulations of Harm-M and Harm-W models demonstrate it is necessary to have large-amplitude along-wind motions to increase the mean generated power. However, in normal operating conditions it is unlikely to achieve these gains. The large-motions condition conflicts with the current design practice of floaters and wind turbines, which tries to place the structure natural frequencies away from the wave spectrum to reduce mechanical loads, reduce the material usage and increase the machine fatigue life.

3.5 Power response with stochastic wind and waves

A full picture of the energy conversion process of a floating wind turbine is gained with the Coupled-S and Coupled-C simulations which consider realistic stochastic wind and waves. In our study, the Coupled-C scenario is the most faithful representation of the environmental conditions of the studied sea area since it reproduces the mutual relationship between wind and waves based on recorded met-ocean data.

3.5.1 Relative wind speed and generated power

The time series of generated power of Fig. 9 obtained with the Harm-M model show a higher average when platform undergoes prescribed motion with a steady below-rated wind speed. To understand if the same happens with stochastic wind and waves, in Fig. 13 we look at the time series of generated power (P_g) and rotor-averaged relative wind speed ($V_{r,avg}$) of the IEA 15 MW wind turbine on the VolturnUS with two below-rated wind conditions. Wind and waves are modeled according to the Coupled-

https://doi.org/10.5194/wes-2023-137
Preprint. Discussion started: 2 November 2023

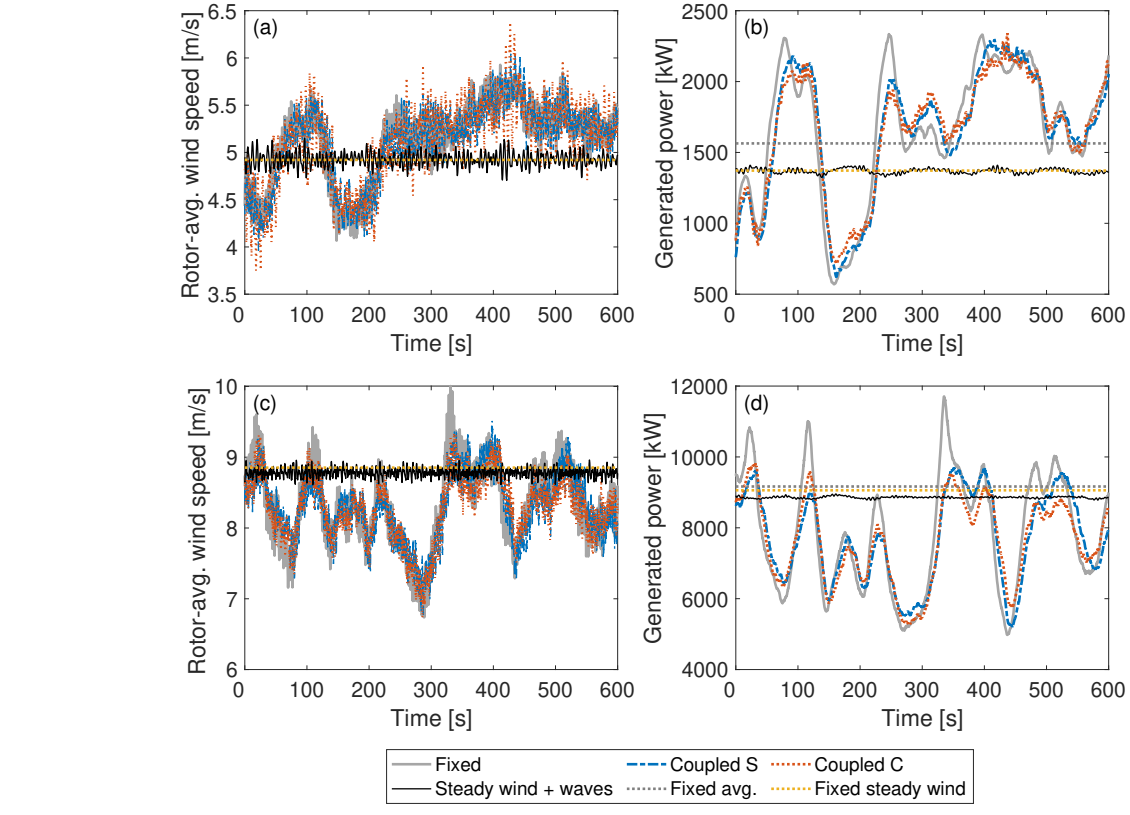

Figure 13. Time series of rotor-averaged relative wind speed and generated power of the IEA 15 MW wind turbine with fixed tower bottom and on top of the VolturnUS semi-submersible. The floating wind turbine is simulated in the Coupled-S and Coupled-C scenarios, with steady wind and the same waves of the Coupled-S case, with steady wind and still water. The fixed turbine case is with the same turbulent wind of the Coupled-S case. **(a), (b)** mean wind speed of 5 m/s, **(c), (d)** mean wind speed of 9 m/s.

370 $V_{\mathrm{r,avg}}$ is an indicator of the energy available for the rotor to be converted in electric power and, as it is shown in Eq. 2-3, its fluctuating component may lead to increased generated power. With waves and steady wind the mean $V_{\mathrm{r,avg}}$ is lower than the nominal average wind speed (i.e., 5 m/s and 9 m/s) due to wind shear and the reduction of rotor area projection on the vertical plane caused by platform tilt. Platform motion driven by waves results in fluctuations of $V_{\mathrm{r,avg}}$ of high frequency and relatively small amplitude. Looking at P_{g}, we see the energy of waves alone is not enough to have a higher mean power than in the fixed
375 case with steady wind.

In cases with stochastic wind, $V_{\mathrm{r,avg}}$ and P_{g} have low-frequency fluctuations which are much larger in amplitude than those associated to wave, and the mean P_{g} is slightly higher than in the steady case. This increment is noticeable at 5 m/s and vanishes for higher wind speeds. For the floating wind turbine with waves, $V_{\mathrm{r,avg}}$ and P_{g} are similar to the fixed case, but with

https://doi.org/10.5194/wes-2023-137
Preprint. Discussion started: 2 November 2023

lower-amplitude positive peaks, thus the average power of the FOWT is slightly lower than for a fixed turbine in equal wind conditions.

3.5.2 Wave directionality and significant height

The effect of wind-wave directionality on the generated power is examined in Fig. 14, which shows the response of the VolturnUS in two simulations of the Coupled-C case that are featured by the same mean wind speed of 6 m/s, very close wave spectra (the only difference is the wave peak period which is 4.6s in one case and 4.7s in the other), but different directions of wind and waves; in one case $[\theta = 135°, \beta = 213°, \gamma = -78°]$, in the other $[\theta = 313°, \beta = 310°, \gamma = 3°]$.

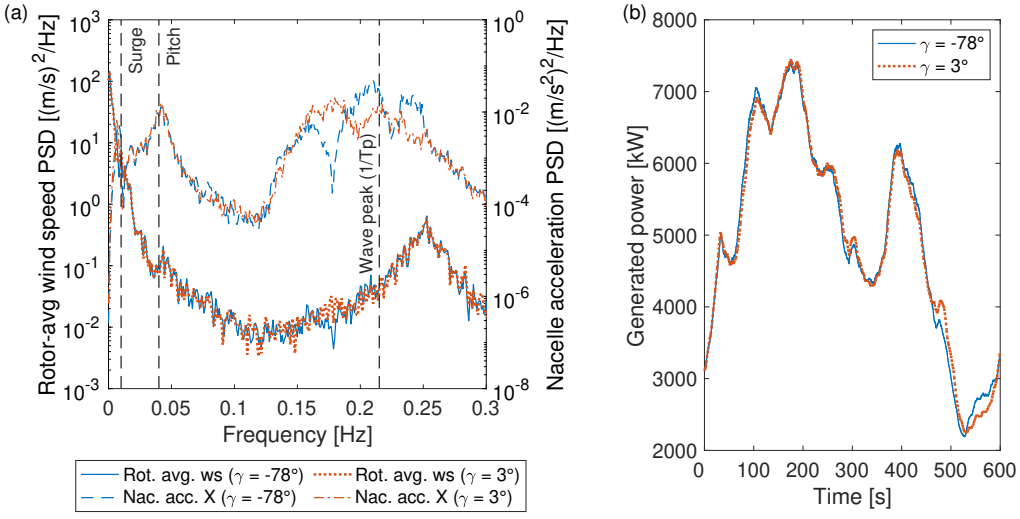

Figure 14. Influence of wind-wave directionality on the power generated by the IEA 15 MW on top of the VolturnUS semi-submersible with a mean wind speed of 6 m/s in the Coupled-C model. **(a)** power spectral density (PSD) of rotor-averaged relative wind speed and nacelle acceleration in the along-wind direction, **(b)** time series of generated power.

The energy associated with wave excitation is visible in the spectrum of $V_{\mathrm{r,avg}}$, which shows a peak near the wave peak frequency $(1/T_{\mathrm{p}})$. This peak is about two order of magnitude lower than the low-frequency portion of the spectrum, which is driven by turbulence. The wind-wave misalignment influences the FOWT motion and this is testified by the spectrum of the nacelle acceleration in the along-wind direction, which shows a different behavior in correspondence of the wave peak depending on γ. A small difference is visible also in the spectrum of $V_{\mathrm{r,avg}}$ near 0.175Hz, but this has about no effect on the generated power which is driven by low-frequency fluctuations of wind turbulence.

3.5.3 Site-specific power curves and AEP

Information about power generated by each floating wind turbine is summarized with a site-specific power curve computed with the algorithm described in Appendix C.

https://doi.org/10.5194/wes-2023-137
Preprint. Discussion started: 2 November 2023

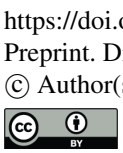

eawe european academy of wind energy
Open Access WIND ENERGY SCIENCE DISCUSSIONS

395 Figure 15 shows the site-specific power curves of the NREL 5 MW and IEA 15 MW wind turbines with a fixed, a semi-submersible, and a spar foundations, that were obtained from Coupled-S and Coupled-C simulations; the fixed case uses the same turbulent wind of the spar and semi-submersible cases and the same control strategy of the floating wind turbines; the steady-state case of the fixed turbine with peak shaving, reported from Fig. 7, serves as a reference of the wind turbine performance when wind is modeled as uniform and steady.

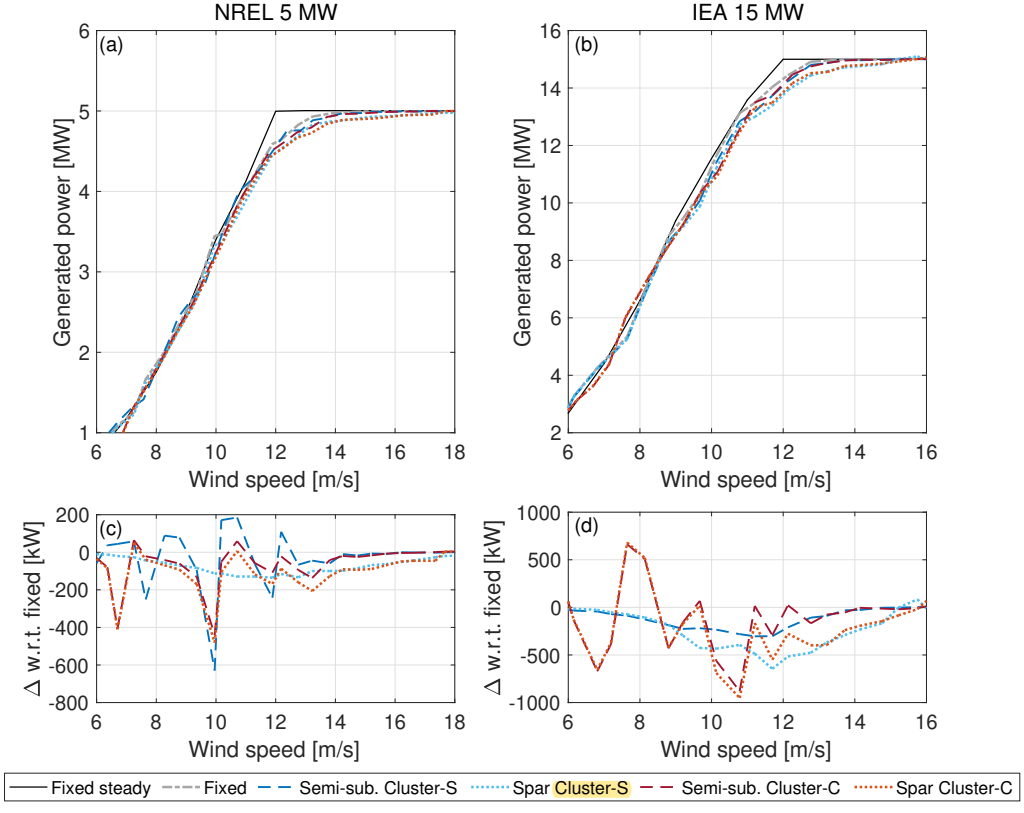

Figure 15. Site-specific power curves of the NREL 5 MW and IEA 5 MW wind turbines with a fixed, a semi-submersible, and a spar foundations. **(a), (b)** power curves obtained in Coupled-S and Coupled-C simulations with stochastic wind and irregular waves, except for the "Fixed steady-state" ones, which are reported from Fig. 7 as a reference of the turbine performance in steady wind. **(c), (d)** variations of the power generated in a floating case compared to a fixed tower-base case.

400 Power curves of turbulent wind cases are below the steady power curve for wind speeds in the upper end of the partial load region and the maximum difference is seen in correspondence of the rated wind speed. The lower power production in turbulent wind cases is mostly due to wind shear which reduces the average wind speed across the rotor, as shown in Sect. 3.2., and it is not considered in the steady power curve. Near the rated wind speed, the turbine controller acts on the blades pitch to counteract rotor overspeed driven by wind gusts. Since the controller does not react instantly to rotor speed and blade pitch

https://doi.org/10.5194/wes-2023-137
Preprint. Discussion started: 2 November 2023

cannot go below 0°, the average blade pitch with turbulence and a near-rated wind speed is different from its power-optimal value which is instead used in the steady wind case.

With a floating foundation and stochastic waves the power curve is generally lower than in the fixed case, especially in the below rated region, and this is ascribed to the platform tilt. Indeed, the power loss with respect to the fixed case increases across the partial-load region with the same trend of the turbine thrust curve (see Fig. 3) and becomes negligible in the full-load region, where rotor thrust decreases and the turbine power is saturated at the wind turbine nameplate capacity. The largest decrement is in proximity of the rated wind speed, where the turbine is more sensitive to blade pitch.

The Coupled-C power curves deviates more from the fixed condition than those obtained in the Coupled-S simulations, especially in low wind speeds. In some wind speed bins, the Coupled-C power curves are above the fixed case, but this is attributed to the methodology for computing the site-specific power curve rather than the wind turbine response that is not expected to change suddenly in contiguous wind speed bins (e.g., the power curve of the 15 MW semi-submersible obtained from the Coupled-C model is above the fixed case at 8.5 m/s and below at 9 m/s). Although we have not analyzed the sensitivity of the power curve to the number of clusters, we expect these oscillations to be smaller if the number of simulations is increased and if the environmental conditions are extracted from a larger dataset covering more uniformly the wind speed operating range of the two turbines.

The two spar FOWTs reach the rated power at a higher wind speed than the semi-submersibles. This behavior is consistent in Coupled-S and Coupled-C simulations and it is ascribed to the nacelle-velocity feedback controller. Near the rated wind speed, the nacelle controller is activated to stabilize platform motion at the expense of a lower efficiency.

Variations of the power curve due to uncertainty in the shear exponent and turbulence intensity are comparable to the power loss of the VolturnUS with respect to the bottom-fixed IEA 15 MW when stochastic wind and waves are considered (see Fig. 15). A recent study of Wiley et al. (2023) shows that turbulent wind speed standard deviation is the single parameter with the highest impact on rotor loads and global motions for the DeepCwind semi-submersible, confirming that a detailed knowledge of the wind environment is needed when assessing the response of floating wind turbines.

The AEP values of the four FOWTs with different modeling of wind and waves are reported in Fig. 16. In all cases the energy production with a floating foundation and the presence of waves is lower than in the fixed-bottom case. The WPRO analysis shows the increment of generated power due to wave-driven motion is around 0.1% for a typical wave spectrum and this small gain is not enough to offset the power loss due to platform tilt caused by thrust and platform compliance. The AEP obtained from simulations with wind-wave misalignment (Coupled-C) is very close to the case with aligned wind and waves (Coupled-S). The small differences are attributed to the AEP estimation algorithm rather than a different physics of the power conversion process of the floating wind turbines, as already observed regarding the power curves of Fig. 15.

https://doi.org/10.5194/wes-2023-137
Preprint. Discussion started: 2 November 2023

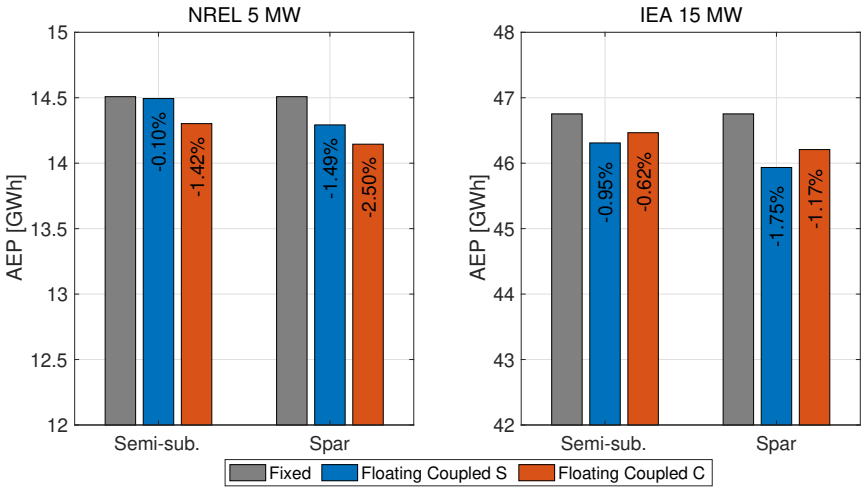

Figure 16. Annual energy production (AEP) of the NREL 5 MW and IEA 5 MW wind turbines obtained with a fixed foundation and turbulent wind, with semi-submersible and spar foundations from the Coupled-S and Coupled-C simulation scenarios. The percent variation of AEP with respect to the fixed case is reported on top of the bars.

The dataset at our disposal covers a time span shorter than what is normally considered in the energy assessment of a wind power plant; wind speed values are low for an area generally seen as quite favorable for the development of floating wind projects, possibly due to the Marignane weather station being located onshore. This is likely to affect the AEP value that may underestimate the true energy potential of the sea site. However, our interest was primarily in understanding the impact of waves on energy production. The dataset covers a winter period when waves are generally stronger, thus conclusion are expected to be valid also if a larger dataset is analyzed.

4 Conclusions

A floating wind turbine rotor normally undergoes large movements permitted by the platform compliance and it may operate differently than with a fixed foundation with possible consequences on the energy capture. Moreover, waves introduce energy in the system forcing the floater which can potentially increase the generated power.

To understand how waves and platform dynamics impact the power production of a floating wind turbine we carried out multi-physics simulations of four turbines of 5-15 MW with spar and semi-submersible support structures. We used four simulation models of increasing complexity that gradually move from simple analytical calculations to a non-linear aero-servo-hydro-elastic model reproducing a realistic scenario with stochastic wind and waves in the Mediterranean Sea.

The main findings of this research are:

1. large along-wind motions can increase the rotor power, but these movements are prevented by the current design philosophy of semi-submersible and spar platforms;

https://doi.org/10.5194/wes-2023-137
Preprint. Discussion started: 2 November 2023

eawe european academy of wind energy
Open Access WIND ENERGY SCIENCE DISCUSSIONS

2. the energy production of the floating wind turbines examined in this study is lower than for a fixed turbine in equal wind conditions;

3. wind modeling is more important than wave modeling for correct estimation of a floating wind turbine power production, at least for a site with met-ocean conditions similar to the one we considered here.

Concerning the first finding, we have shown the wind turbine controller action makes power gains due to wave-driven motion possible only in below-rated winds speeds. The increment in power is proportional to the amplitude and frequency of platform movement and it is maximum when the rotor moves in the along wind direction. Instead, with wind-wave misalignment, part of the wave energy is used to excite cross-wind motions that do not contribute to increasing the energy of the flow available for the rotor to be converted in electric power. Taking into account the hydrodynamic loads and the platform dynamic response we see wave excitation is generally not strong enough to achieve the large movements required to have a significant rise of generated power. Large and high-frequency motions are needed to increase the wind turbine power output, but they would cause high structural loads. This is in conflict with the design objectives of the platforms we examined which aim to reduce material usage and extend as much as possible the fatigue life of the system.

Concerning the second finding, the lower performance of a floating wind turbine compared to a bottom-fixed one is due to: the use of wind turbine control strategies that mitigate structural loads sacrificing energy conversion efficiency, wind turbulence and shear, and the static tilt of the floater caused by the combination of thrust force and high compliance of floating foundations. It should be verified if these results obtained for spar-buoy and semi-submersible wind turbines are also valid for tension-leg platform (TLP) systems, which tend to have higher frequency and smaller amplitude motions.

About the third finding, we realized that information about wind parameters, such as shear and turbulence, might be scarce in the early stage of floating wind projects and this lack of data should be addressed properly when evaluating the energy potential of a floating wind plant. At the same time, the energy evaluation process can be simplified considering a reduced number of wave conditions. Future work should prove if this is true also for sites characterized by different environmental parameters (e.g., stronger waves).

A wind turbine power curve is influenced significantly by the wind turbine control strategy and floater restoring characteristics which must be modeled in energy calculations. This is important for the individual machines, but also for wind farm modeling, where the power curve is often used in engineering tools as a simplified representation of the turbine response (e.g., in FLOw Redirection and Induction at Steady state FLORIS (NREL (2023))).

As we have shown, exploiting the energy of waves with the current technology of semis-submersible and spar-buoy systems is not possible. Future designs may explore the trade-off between loads and increased power and see if it is feasible to leverage the peculiar physics of a floating rotor to harvest more energy and further decrease the cost of floating wind.

Data availability. The OpenFAST models of the DeepCwind and OC3 floating wind turbines are available at https://github.com/OpenFAST/r-test/tree/main/glue-codes/openfast. The OpenFAST model of the VolturnUS can be downloaded from https://github.com/IEAWindTask37/IEA-

https://doi.org/10.5194/wes-2023-137
Preprint. Discussion started: 2 November 2023

eawe european academy of wind energy
Open Access WIND ENERGY SCIENCE DISCUSSIONS

15-240-RWT/tree/master/OpenFAST. The OpenFAST model of the WindCrete can be found at https://zenodo.org/record/4322446 (Molins et al. (2020)). The dataset of met-ocean conditions and the programs used for its analysis can be obtained contacting the authors.

https://doi.org/10.5194/wes-2023-137
Preprint. Discussion started: 2 November 2023

eawe european academy of wind energy
Open Access WIND ENERGY SCIENCE DISCUSSIONS

Appendix A: Example of KMA clustering

The K-means algorithm introduced in Sect. 2.1.4 is applied to the dataset of the Golf de Fos site presented in Sect. 2.3 to extract $M = 5$ clusters. The number of clusters used in this example is lower than in Coupled-C simulations, where $M = 36$, to facilitate interpretation of the result.

Figure A1 shows the KMA output. Each dot is one of the 3362 conditions in the dataset represented in the five-dimensional space $\mathbf{x} = \{U, \beta, H_s, T_p, \theta\}$. Dots are colored according to the cluster to which they are assigned by the KMA. As visible, dots of the same color share similar features, for example yellow dots are sea states with: $\beta = [250° - 50°]$, $\theta = [270° - 50°]$. In the KMA, each cluster is represented by its centroid, marked by a $\times$.

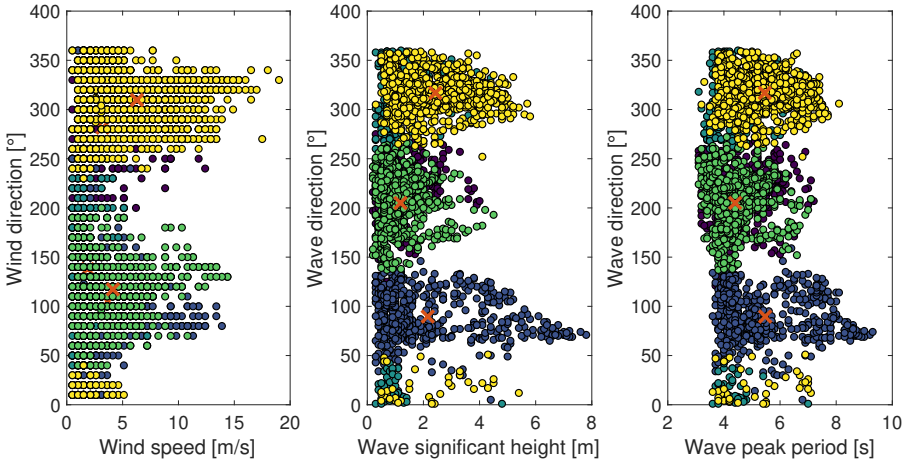

Figure A1. Met-ocean data (wind speed, wind direction, wave significant height, wave peak period, wave direction) of the Gulf de Fos site are divided into clusters with the K-means algorithm. Datapoints are colored according to the cluster to which they are assigned and clusters centroids are marked by the $\times$.

As we see, if the number of clusters is too low, as in this example, centroids do not represent accurately the dataset features. In the yellow cluster there is no distinction of wind speed, wave height or wave period, which span a large range and sometimes are quite far from those of the cluster centroid.

Appendix B: Wind and wave conditions from clustering

The environmental conditions of Coupled-S simulations are summarized in Table B1 and those of Coupled-C simulations in Table B2.

https://doi.org/10.5194/wes-2023-137
Preprint. Discussion started: 2 November 2023

eawe european academy of wind energy
Open Access WIND ENERGY SCIENCE DISCUSSIONS

Table B1. Wind and wave conditions of the Coupled-S simulations ("w. s." is wind speed).

Case ID	Mean w. s. [m/s]	Wave height [m]	Wave period [s]
1	3.0	1.2	5.0
2	3.0	1.2	6.0
3	3.0	1.2	4.0
4	5.0	1.5	5.0
5	5.0	1.5	6.0
6	5.0	1.5	4.0
7	7.0	1.7	6.0
8	7.0	1.7	5.0
9	7.0	1.7	7.0
10	9.0	2.0	6.0
11	9.0	2.0	5.0
12	9.0	2.0	7.0
13	11.0	2.3	6.0
14	11.0	2.3	7.0
15	11.0	2.3	5.0
16	13.0	2.5	6.0
17	13.0	2.5	7.0
18	13.0	2.5	8.0
19	15.0	2.8	6.0
20	15.0	2.8	7.0
21	15.0	2.8	8.0
22	17.0	3.0	7.0
23	17.0	3.0	6.0
24	17.0	3.0	8.0
25	19.0	3.3	7.0
26	19.0	3.3	6.0
27	19.0	3.3	8.0
28	21.0	3.5	7.0
29	21.0	3.5	8.0
30	21.0	3.5	9.0
31	23.0	3.8	7.0
32	23.0	3.8	8.0
33	23.0	3.8	9.0
34	25.0	4.0	7.0
35	25.0	4.0	8.0
36	25.0	4.0	9.0

https://doi.org/10.5194/wes-2023-137
Preprint. Discussion started: 2 November 2023

eawe european academy of wind energy
Open Access WIND ENERGY SCIENCE DISCUSSIONS

Table B2. Wind and wave conditions identified by means of K-means clustering and used for the Coupled-C simulations ("w. s." is wind speed, "Count" is the number of datapoints in each cluster).

Cluster ID	Mean w. s. [m/s]	Wind direction [°]	Wave height [m]	Wave period [s]	Wave direction [°]	Count [–]
1	3.0	137	0.8	4.0	273	69
2	3.0	257	1.0	4.2	342	65
3	3.0	11	1.6	4.8	298	55
4	3.0	148	0.7	4.4	79	38
5	3.5	256	0.6	3.7	229	77
6	3.5	268	0.9	4.4	172	70
7	4.0	203	1.2	4.9	209	63
8	4.0	141	0.7	4.1	118	50
9	4.0	269	1.1	4.2	302	60
10	4.0	352	1.4	4.6	337	96
11	4.0	317	1.3	4.6	239	50
12	4.5	71	0.9	4.3	135	55
13	4.5	75	1.2	4.8	82	27
14	4.5	118	1.5	5.0	71	70
15	4.5	127	0.6	3.9	168	98
16	4.5	343	6.0	8.2	74	24
17	5.0	348	3.6	6.4	32	42
18	5.5	350	3.3	6.2	324	46
19	5.5	85	1.4	4.7	225	124
20	6.0	135	1.4	4.7	213	111
21	6.0	313	1.4	4.6	310	142
22	6.0	93	0.9	4.1	191	105
23	6.5	316	2.9	5.9	313	49
24	6.5	310	1.5	4.7	351	68
25	6.5	74	3.8	7.1	108	102
26	8.5	104	1.8	5.2	107	73
27	9.0	273	1.6	5.3	224	53
28	9.5	270	2.1	5.5	269	50
29	10.0	284	1.9	5.0	313	123
30	11.5	126	1.4	4.5	186	47
31	13.0	86	5.3	7.8	85	114
32	13.0	298	3.0	5.9	315	127
33	13.5	319	2.1	5.2	316	28
34	15.5	280	4.1	6.8	302	49
35	15.5	141	2.9	5.9	178	56
36	17.5	325	3.9	6.6	316	135

https://doi.org/10.5194/wes-2023-137
Preprint. Discussion started: 2 November 2023

eawe european academy of wind energy
Open Access WIND ENERGY SCIENCE DISCUSSIONS

Appendix C: Wind and wave conditions from clustering

The site-specific power curve and the AEP are derived according to the algorithm of the IEC 61400-12 standard (International Electrotechnical Commission (2022)) based on time series of hub-height wind speed and generated power.

Time series of wind speed and generated power are divided into 10 min segments and, for each segment, the mean value is computed. The dataset of 10 min-mean values is sorted using the method of bins:

1. the wind speed range is divided in 0.5 m/s contiguous bins centered on multiples of 0.5 m/s and the dataset is distributed inside the bins according to the 10 min-mean wind speed;

2. the dataset must cover a wind speed range extending from 1 m/s below cut-in to 1.5 time the wind speed at 85% of the wind turbine rated power. Otherwise, for pitch-controlled wind turbines as the NREL 5 MW and the IEA 15 MW, the power curve is considered complete when the rated power is reached and the average power does not change by more than 0.5% of the power, or 5 kW, for three consecutive wind speed bins. If the power curve does not include data up to cut-out wind speed, the power curve is extrapolated from the maximum complete wind speed to cut-out wind speed;

3. the dataset is considered complete when each bin includes a minimum of 30 min of sampled data. For incomplete bins, the bin value is estimated by linear interpolation from the two adjacent complete bins.

The power curve (i.e., power as a function of wind speed) is determined based on the hub-height wind speed of each bin:

$$V_i = \frac{1}{N_i} \sum_{j=1}^{N_i} V_{n,i,j} \,, \tag{C1}$$

where V_i is the average wind speed in bin i, $V_{n,i,j}$ is the wind speed of the data point j in bin i, N_i is the number of 10 min data points in the bin i. The power of each bin is:

$$P_i = \frac{1}{N_i} \sum_{j=1}^{N_i} P_{n,i,j} \,, \tag{C2}$$

where P_i is the average power in bin i, $P_{n,i,j}$ is the power of the data point j in bin i, N_i is the number of 10 min data points in bin i. An example of power curve obtained with the method of bins is reported in Fig. C1.

https://doi.org/10.5194/wes-2023-137
Preprint. Discussion started: 2 November 2023

eawe european academy of wind energy
Open Access WIND ENERGY SCIENCE DISCUSSIONS

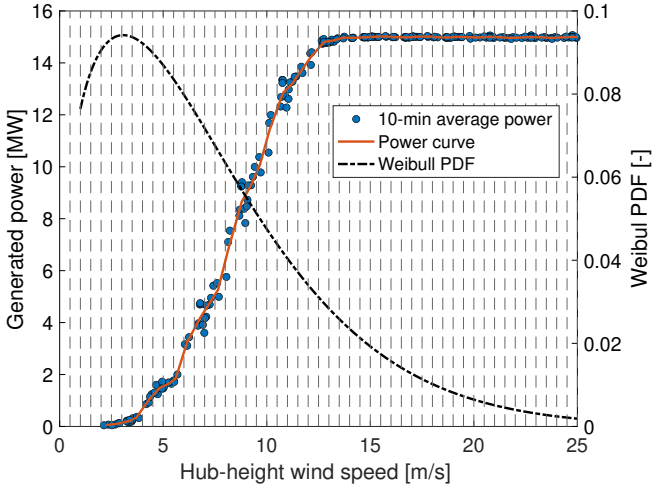

Figure C1. Construction of the site-specific power curve from simulations of the Coupled-S or Coupled-C scenarios. Time series of generated power obtained from OpenFAST simulations are divided into 10 min sub-histories and dots are the corresponding mean values.

The AEP is evaluated combining the power curve obtained with the method of bins with the wind speed frequency distribution as:

$$\mathrm{AEP} = N_h \sum_{i=1}^{N} (F(V_i) - F(V_{i-1})) \left(\frac{P_{i-1} + P_i}{2} \right), \tag{C3}$$

Where AEP is the annual energy production, $N_h = 8760$ is the number of hours in one year, N is the number of bins, V_i is the average wind speed in bin i, P_i is the average power of bin i, $F(V_i)$ is the site-specific Weibull cumulative probability distribution function for wind speed (i.e., the one of Fig. 5 in the case of this paper). The summation in Eq. C3 is initiated setting $F(V_{i-1}) = V_i - 0.5$ and $P_{i-1} = 0$.

Author contributions. AF contributed to conceptualization, investigation, methodology, software, visualization, and writing – original draft preparation. GC contributed to conceptualization, investigation, methodology, software, and writing – original draft preparation. MDP contributed to methodology, investigation, software, and writing – original draft preparation. SM contributed to supervision, project administration, and writing – review and editing. MB contributed to conceptualization, funding acquisition, supervision, and writing – review and editing.

Competing interests. The authors declare that they have no conflict of interest.

https://doi.org/10.5194/wes-2023-137
Preprint. Discussion started: 2 November 2023

eawe european academy of wind energy
Open Access WIND ENERGY SCIENCE DISCUSSIONS

References

Abbas, N. J., Zalkind, D. S., Pao, L., and Wright, A.: A reference open-source controller for fixed and floating offshore wind turbines, Wind Energy Science, 7, 53–73, https://doi.org/10.5194/wes-7-53-2022, https://wes.copernicus.org/articles/7/53/2022/, 2022.

Allen, C., Viselli, A., Dagher, H., Goupee, A., Gaertner, E., Abbas, N., Hall, M., and Barter, G.: Definition of the UMaine VolturnUS-S Reference Platform Developed for the IEA Wind 15-Megawatt Offshore Reference Wind Turbine, Technical Report NREL/TP-5000-76773, https://www.nrel.gov/docs/fy20osti/76773.pdf, Available at https://www.nrel.gov/docs/fy20osti/76773.pdf, 2020.

Amaral, R., Laugesen, K., Masciola, M., von Terzi, D., Deglaire, P., and Viré, A.: A frequency-time domain method for annual energy production estimation in floating wind turbines, Journal of Physics: Conference Series, 2265, 042 025, https://doi.org/10.1088/1742-6596/2265/4/042025, https://dx.doi.org/10.1088/1742-6596/2265/4/042025, 2022.

Arthur, D. and Vassilvitskii, S.: K-Means++: The Advantages of Careful Seeding, in: Proceedings of the Eighteenth Annual ACM-SIAM Symposium on Discrete Algorithms, SODA '07, p. 1027–1035, Society for Industrial and Applied Mathematics, USA, 2007.

Campos, A., Molins, C., Gironella, X., and Trubat, P.: Spar concrete monolithic design for offshore wind turbines, Proceedings of the Institution of Civil Engineers - Maritime Engineering, 169, 49–63, https://doi.org/10.1680/jmaen.2014.24, https://doi.org/10.1680/jmaen.2014.24, 2016.

Camus, P., Mendez, F. J., Medina, R., and Cofiño, A. S.: Analysis of clustering and selection algorithms for the study of multivariate wave climate, Coastal Engineering, 58, 453–462, https://doi.org/https://doi.org/10.1016/j.coastaleng.2011.02.003, https://www.sciencedirect.com/science/article/pii/S0378383911000354, 2011.

Clifton, A., Daniels, M. H., and Lehning, M.: Effect of winds in a mountain pass on turbine performance, Wind Energy, 17, 1543–1562, https://doi.org/https://doi.org/10.1002/we.1650, https://onlinelibrary.wiley.com/doi/abs/10.1002/we.1650, 2014.

Cottura, L., Caradonna, R., Novo, R., Ghigo, A., Bracco, G., and Mattiazzo, G.: Effect of pitching motion on production in a OFWT, Journal of Ocean Engineering and Marine Energy, 8, 319 – 330, https://doi.org/10.1007/s40722-022-00227-0, https://www.scopus.com/inward/record.uri?eid=2-s2.0-85132638963&doi=10.1007%2fs40722-022-00227-0&partnerID=40&md5=ad3684f562590d9cf27f6c7ca5c64a95, 2022.

EMODnet: EMODnet Bathymetry World Base Layer, https://emodnet.ec.europa.eu/en/bathymetry, 2023.

France, M.: Mètéo-France. Gulf de Lion buoy, https://donneespubliques.meteofrance.fr/?fond=produit{&}id{_}produit=95{&}id{_}rubrique=32, 2022.

Gaertner, E., Rinker, J. and. Sethuraman, L., Zahle, F., Anderson, B., Barter, G., Abbas, N., Meng, F., Bortolotti, P., Skrzypinski, W., Scott, G., Feil, R., Bredmose, H., Dykes, K., Shields, M., Allen, C., and Viselli, A.: Definition of the IEA 15-Megawatt Offshore Reference Wind Turbine, Tech. rep., National Renewable Energy Laboratory, https://www.nrel.gov/docs/fy20osti/75698.pdf, Available at https://www.nrel.gov/docs/fy20osti/75698.pdf, 2020.

Hasselmann, K. F., Barnett, T. P., Bouws, E., Carlson, H. C., Cartwright, D. E., Enke, K., Ewing, J. A., Gienapp, H., Hasselmann, D. E., Kruseman, P., Meerburg, A., Müller, P. M., Olbers, D. J., Richter, K., Sell, W., and Walden, H.: Measurements of wind-wave growth and swell decay during the Joint North Sea Wave Project (JONSWAP), 1973.

International Electrotechnical Commission: Wind energy generation systems - Part 3-1: Design requirements for fixed offshore wind turbines, IEC 61400-3-1:2019, Tech. Rep. IEC 61400-12-1:2022, International Electrotechnical Commission, https://webstore.iec.ch/publication/29360, 2019.

https://doi.org/10.5194/wes-2023-137
Preprint. Discussion started: 2 November 2023

International Electrotechnical Commission: Wind energy generation systems - Part 12-1: Power performance measurements of electricity producing wind turbines, IEC 61400-12-1:2022, Tech. Rep. IEC 61400-12-1:2022, International Electrotechnical Commission, https://webstore.iec.ch/publication/68499#additionalinfo, 2022.

Jonkman, J.: Definition of the Floating System for Phase IV of OC3, NREL/TP-500-47535, https://www.nrel.gov/docs/fy10osti/47535.pdf, Available at https://www.nrel.gov/docs/fy10osti/47535.pdf, 2009.

Jonkman, J., Butterfield, S., Musial, W., and Scott, G.: Definition of a 5-MW reference wind turbine for offshore system development, NREL/TP-500-38060, https://www.nrel.gov/docs/fy09osti/38060.pdf, Available at https://www.nrel.gov/docs/fy09osti/38060.pdf, 2009.

Mahfouz, M. Y., Molins, C., Trubat, P., Hernández, S., Vigara, F., Pegalajar-Jurado, A., Bredmose, H., and Salari, M.: Response of the International Energy Agency (IEA) Wind 15 MW WindCrete and Activefloat floating wind turbines to wind and second-order waves, Wind Energy Science, 6, https://doi.org/10.5194/wes-6-867-2021, https://wes.copernicus.org/articles/6/867/2021/, 2021.

Martini, M., Guanche, R., Armesto, J. A., Losada, I. J., and Vidal, C.: Met-ocean conditions influence on floating offshore wind farms power production, Wind Energy, 19, 399–420, https://doi.org/https://doi.org/10.1002/we.1840, https://onlinelibrary.wiley.com/doi/abs/10.1002/we.1840, 2016.

Meteostat: Marseille - Marignane weather station, https://meteostat.net/en/station/07650?t=2023-06-12/2023-06-19, 2022.

Molins, C., Trubat, P., and Mahfouz, M. Y.: UPC - WINDCRETE OpenFAST model 15MW FOWT - Grand Canary Island, https://doi.org/10.5281/zenodo.4322446, https://doi.org/10.5281/zenodo.4322446, 2020.

NREL: FLORIS, https://github.com/NREL/floris, 2023.

Robertson, A., Jonkman, J., Masciola, M., Song, H., Goupee, A., Coulling, A., and Luan, C.: Definition of the Semisubmersible Floating System for Phase II of OC4, NREL/TP-5000-60601, https://www.nrel.gov/docs/fy14osti/60601.pdf, Available at https://www.nrel.gov/docs/fy14osti/60601.pdf, 2014.

Schelbergen, M., Kalverla, P. C., Schmehl, R., and Watson, S. J.: Clustering wind profile shapes to estimate airborne wind energy production, Wind Energy Science, 5, 1097–1120, https://doi.org/10.5194/wes-5-1097-2020, https://wes.copernicus.org/articles/5/1097/2020/, 2020.

St. Martin, C. M., Lundquist, J. K., Clifton, A., Poulos, G. S., and Schreck, S. J.: Wind turbine power production and annual energy production depend on atmospheric stability and turbulence, Wind Energy Science, 1, 221–236, https://doi.org/10.5194/wes-1-221-2016, https://wes.copernicus.org/articles/1/221/2016/, 2016.

van der Veen, G. J., Couchman, I. J., and Bowyer, R. O.: Control of floating wind turbines, in: 2012 American Control Conference (ACC), pp. 3148–3153, https://doi.org/10.1109/ACC.2012.6315120, 2012.

van Kuik, G. A. M., Peinke, J., Nijssen, R., Lekou, D., Mann, J., Sørensen, J. N., Ferreira, C., van Wingerden, J. W., Schlipf, D., Gebraad, P., Polinder, H., Abrahamsen, A., van Bussel, G. J. W., Sørensen, J. D., Tavner, P., Bottasso, C. L., Muskulus, M., Matha, D., Lindeboom, H. J., Degraer, S., Kramer, O., Lehnhoff, S., Sonnenschein, M., Sørensen, P. E., Künneke, R. W., Morthorst, P. E., and Skytte, K.: Long-term research challenges in wind energy – a research agenda by the European Academy of Wind Energy, Wind Energy Science, 1, 1–39, https://doi.org/10.5194/wes-1-1-2016, https://wes.copernicus.org/articles/1/1/2016/, 2016.

Wiley, W., Jonkman, J., Robertson, A., and Shaler, K.: Sensitivity Analysis of Numerical Modeling Input Parameters on Floating Offshore Wind Turbine Loads, Wind Energy Science Discussions, 2023, 1–35, https://doi.org/10.5194/wes-2023-49, https://wes.copernicus.org/preprints/wes-2023-49/, 2023.

Wiser, R., Rand, J., Seel, J., Beiter, P., Baker, E., Lantz, E., and Gilman, P.: Expert elicitation survey predicts 37% to 49% declines in wind energy costs by 2050, Nature Energy, 6, 555–565, https://doi.org/https://doi.org/10.1038/s41560-021-00810-z, https://doi.org/10.1038/s41560-021-00810-z, 2021.